

Deep Learning-Based Survival Analysis with Copula-Based Activation Functions for Multivariate Response Prediction

Jong-Min Kim

Statistics Discipline, Division of Science and Mathematics, University of Minnesota-Morris, Morris, MN 56267, USA

EGADE Business School, Tecnológico de Monterrey, Ave. Rufino Tamayo, Garza Garcia, NL, CP. 66269, Mexico

Il Do Ha

Department of Statistics and Data Science, Pukyong National University, Busan, South Korea

Sangjin Kim¹

Department of Management Information Systems, Dong-A University, Busan, South Korea

Summary

This research integrates deep learning, copula functions, and survival analysis to effectively handle highly correlated and right-censored multivariate survival data. It introduces copula-based activation functions (Clayton, Gumbel, and their combinations) to model the nonlinear dependencies inherent in such data. Through simulation studies and analysis of real breast cancer data, our proposed CNN-LSTM with copula-based activation functions for multivariate multi-types of survival responses enhances prediction accuracy by explicitly addressing right-censored data and capturing complex patterns. The model's performance is evaluated using Shewhart control charts, focusing on the average run length (ARL).

Keywords: Multivariate survival data, Copula, deep learning, control chart.

1 Introduction

Long Short-Term Memory (LSTM) networks are a specialized type of recurrent neural network (RNN) designed to address the vanishing gradient problem that often arises during the training of deep neural networks. Introduced by Sepp Hochreiter and Jürgen Schmidhuber in 1997 [1], LSTMs have become widely used in time series analysis and sequential data processing, with applications in speech recognition, financial modeling, and natural language processing. In parallel, Convolutional Neural Networks (CNNs), pioneered by Yann LeCun with the LeNet-5 architecture in the late 1980s and early 1990s [2], have been instrumental in computer vision tasks, such as image classification and object detection.

¹*Corresponding Author:* Sangjin Kim, Department of Management Information Systems, Dong-A University, Busan, South Korea, Email: skim10@dau.ac.kr

This research integrates deep learning models (CNN-LSTM and LSTM), copula functions, and survival analysis to address the challenges posed by highly correlated, right-censored multivariate survival data [3]. Survival data often involve multiple correlated variables-such as time-to-event outcomes and covariates-observed across different subjects or response types [4, 5]. While deep learning models offer powerful alternatives to traditional methods, standard activation functions such as ReLU [6] and sigmoid [7] may fail to capture complex inter-variable dependencies [8].

Previous work has explored univariate time-to-event prediction using neural networks and Cox regression [9]. Copula functions are particularly well-suited for modeling multivariate dependencies [10, 11], making them valuable in survival analysis [12–15]. More recently, [16] introduced copula-based deep neural networks for multivariate survival data with clustered responses, assuming fixed copula dependence parameters. However, their study did not demonstrate the benefits of using Clayton copula-based activation functions in survival prediction.

In this work, we extend the existing literature by incorporating learnable copula-based activation functions-specifically Clayton, Gumbel, and their combinations-to better model nonlinear dependencies in multivariate survival outcomes. The proposed CNN-LSTM copula model improves prediction performance by explicitly addressing right-censored data and capturing intricate survival patterns. Model performance is evaluated using Shewhart control charts, with a particular focus on the Average Run Length (ARL) metric [17].

The remainder of this paper is organized as follows: Section 2 reviews the gap between classical survival analysis and machine learning approaches. Section 3 introduces the deep learning architecture and the learnable copula-based activation functions. Sections 4 and 5 present empirical results using both simulated and real-world breast cancer data. Finally, Section 6 summarizes our findings and discusses their broader implications.

2 Bridging the Gap Between Machine Learning and Classical Survival Analysis

Traditional survival models, such as the Cox proportional hazards model [18], assume linear relationships between input-output variables or proportional hazards, which limits their effectiveness on complex or high-dimensional datasets. Similarly, the Kaplan–Meier estimator [19] does not incorporate covariates, limiting its applicability to nuanced, real-world survival data.

To address these limitations, our research employs CNN-LSTM models, which are well-suited to capturing nonlinear, time-dependent relationships between input-output in survival data. CNNs excel at extracting spatial or structural features, while LSTMs are proficient in modeling long-term

temporal dependencies. Their integration enables the CNN-LSTM architecture to jointly learn rich feature representations and dynamic survival patterns such as local dependence or nonlinear interaction in time-to-event outcomes, offering a more flexible and accurate alternative to traditional models.

A key innovation in our study is the introduction of copula-based activation functions—specifically Clayton, Gumbel, and their combinations—within the deep survival modeling framework. Copulas are powerful tools for modeling nonlinear dependencies between multiple correlated survival responses, overcoming the independence assumptions often inherent in traditional models. Clayton copula activation functions are effective in capturing asymmetric lower tail dependence (e.g., extreme early failures), while Gumbel copulas capture upper tail dependence (e.g., simultaneous late failures) [10, 11]. These copula activations allow the network to learn more realistic joint distributions among event times. In medical settings, survival times for multiple events are often correlated—for instance, in multi-organ failure, recurrent infections or disease progression across different systems. Traditional models rarely account for such dependencies explicitly. Copula-based models, by contrast, provide a principled way to capture and model these interdependencies, enhancing prediction performance and clinical interpretability.

To evaluate our approach, we simulate realistic survival data with censoring and inter-event correlation. The simulated data incorporate Weibull-distributed survival times, which more closely reflect empirical survival behaviors than Gaussian or exponential distributions. This setup enables us to assess model robustness under varying censoring rates and validate performance in a controlled environment prior to applying the model to real-world data.

A core strength of our method is its capacity to explicitly handle right-censored data—a ubiquitous issue in survival analysis. By properly incorporating censoring mechanisms into the training process, we mitigate bias arising from incomplete observations. The CNN-LSTM copula model thus delivers improved accuracy and robustness in survival prediction tasks involving complex, correlated, and censored data.

While recent developments have emphasized neural network-based approaches for modeling survival data, it is important to acknowledge the broader landscape of machine learning methodologies that have been applied to survival analysis. In particular, tree-based models and support vector machines (SVMs) have played a significant role and continue to serve as strong alternatives or complements to neural architectures.

Tree-based methods, such as Random Survival Forests (RSF) introduced by Ishwaran et al. [20], extend the classical random forest algorithm to handle right-censored survival data, typically using the log-rank test to split survival trees. RSF is non-parametric, handles non-linearities

and interactions naturally, and can estimate survival functions without requiring proportional hazards assumptions. More recently, gradient boosting techniques have been adapted for survival data—for example, CoxBoost proposed by Binder and Schumacher [21], and adaptations of XGBoost with Cox proportional hazards loss—offering flexible and high-performance solutions in high-dimensional settings.

In parallel, support vector machine (SVM)-based approaches have also been extended to accommodate censored data. For instance, the Survival SVM developed by Van Belle et al. [22] optimizes a ranking-based loss function tailored to censored observations, allowing for margin-based learning of risk scores under partial information constraints.

These machine learning models provide competitive benchmarks and often excel in small-to-moderate sample settings, or where interpretability and model stability are important. A brief comparison of these methods with neural approaches sets the stage for the deeper exploration of deep learning-based survival models that follows.

3 Methods

Survival analysis frequently involves right-censored data, where the event time is not fully observed. This paper proposes a CNN-LSTM model augmented with learnable copula-based activation functions. Unlike approaches using fixed dependency parameters, we estimate the copula parameters dynamically during training to better capture nonlinear dependencies in survival outcomes.

Sequential data modeling is essential in domains such as survival analysis, financial forecasting, and high-frequency volatility modeling. CNNs and LSTMs have been widely used to capture local and long-range dependencies. However, conventional activation functions—such as ReLU, sigmoid, and tanh—fail to account for tail dependence and nonlinear associations in multivariate or censored settings.

To address this issue, we introduce an adaptive copula-based activation framework for CNN-LSTM networks. The key innovations of this paper include: (i) incorporating copula functions as activation mechanisms to explicitly model dependencies between neurons; (ii) using learnable copula-based activations, where the dependence parameters θ are optimized during training; (iii) applying Clayton and Gumbel copulas to capture lower and upper tail dependencies, respectively; and (iv) proposing a hybrid copula-ReLU activation that combines tail dependence modeling with the sparsity benefits of ReLU.

3.1 Copula-Based Activation Functions

Let $x \in \mathbb{R}$ denote a pre-activation input to a neuron. We transform x into the uniform domain via the standard Gaussian cumulative distribution function (CDF), $\Phi(\cdot)$:

$$u = \Phi(x) = \frac{1}{2} \left(1 + \operatorname{erf} \left(\frac{x}{\sqrt{2}} \right) \right),$$

where $\operatorname{erf}(\cdot)$ is the Gaussian error function. The copula-based activation function, denoted by $g_{\text{Copula}}(x, \theta)$, is then defined on $u \in [0, 1]$.

Clayton copula activation (lower tail dependence). The bivariate Clayton copula is:

$$C_\theta(u, v) = \left(u^{-\theta} + v^{-\theta} - 1 \right)^{-\frac{1}{\theta}}, \quad \theta > 0. \quad (1)$$

The Clayton copula-based activation is defined as:

$$g_{\text{Clayton}}(x, \theta) = \left(u^{-\theta} - 1 \right)^{-\frac{1}{\theta}}.$$

Gumbel copula activation (upper tail dependence). The bivariate Gumbel copula is:

$$C_\theta(u, v) = \exp \left(- \left[(-\log u)^\theta + (-\log v)^\theta \right]^{\frac{1}{\theta}} \right), \quad \theta \geq 1. \quad (2)$$

The corresponding activation is:

$$g_{\text{Gumbel}}(x, \theta) = \exp \left(- (-\log u)^\theta \right).$$

Hybrid copula activation. To approximate asymmetric tail dependencies, we define a hybrid activation as the average of Clayton and Gumbel activations:

$$g_{\text{Hybrid}}(x, \theta_C, \theta_G) = \frac{g_{\text{Clayton}}(x, \theta_C) + g_{\text{Gumbel}}(x, \theta_G)}{2}. \quad (3)$$

Copula-ReLU hybrid activation. To enforce non-negativity and induce sparsity, we define:

$$g_{\text{Clayton-ReLU}}(x, \theta) = \max(0, g_{\text{Clayton}}(x, \theta)).$$

The copulas employed-Clayton and Gumbel-are bivariate and applied independently to each output pair. Our current framework involves only two survival responses, so one bivariate copula

suffices per instance. The Clayton copula models lower tail dependence (e.g., early joint failures), while the Gumbel copula captures upper tail dependence (e.g., simultaneous late failures) [10, 11].

The hybrid copula activation in Equation 3 is motivated by the need to capture both types of tail dependence. This mirrors ensemble learning, where aggregating multiple models (here, copulas) improves generalization. The use of ReLU-based copula modifications, such as $g_{\text{Clayton-ReLU}}$, ensures that activations remain non-negative and sparse, aiding interpretability and regularization.

While this approach is empirically grounded, it remains a functional surrogate for a more formal theory of copula-based activation functions. Future directions include establishing theoretical guarantees for universal approximation, Lipschitz continuity, and training stability under such activations. For multivariate outputs, this framework can be extended using pair-copula constructions (PCCs), such as canonical vines (C-vines) or drawable vines (D-vines) [23, 24]. These allow decomposition of high-dimensional copulas into cascades of bivariate structures while preserving interpretability. In this work, we restrict attention to the bivariate case due to computational constraints in deep survival modeling. However, vine copula extensions remain a promising avenue for future work involving more complex interdependent outcomes.

3.2 LSTM Model and CNN-LSTM Model for Multivariate Prediction

An LSTM network consists of memory cells that include three fundamental gating mechanisms: the *forget gate*, which determines which past information should be discarded; the *input gate*, which controls the flow of new information into the memory cell; and the *output gate*, which regulates how much information from the memory cell contributes to the final output.

The updates in an LSTM cell at time step t are given by:

$$\begin{aligned} f_t &= \sigma(W_f x_t + U_f h_{t-1} + b_f), \\ i_t &= \sigma(W_i x_t + U_i h_{t-1} + b_i), \\ \tilde{C}_t &= \tanh(W_c x_t + U_c h_{t-1} + b_c), \\ C_t &= f_t \odot C_{t-1} + i_t \odot \tilde{C}_t, \\ o_t &= \sigma(W_o x_t + U_o h_{t-1} + b_o), \\ h_t &= o_t \odot \tanh(C_t), \end{aligned}$$

where $x_t \in \mathbb{R}^d$ is the input vector at time t , $h_t \in \mathbb{R}^h$ is the hidden state, and $C_t \in \mathbb{R}^h$ is the cell state. The matrices $W. \in \mathbb{R}^{h \times d}$, $U. \in \mathbb{R}^{h \times h}$, and vectors $b. \in \mathbb{R}^h$ represent trainable parameters. The symbol \odot denotes element-wise (Hadamard) multiplication.

The activation function $\sigma(\cdot)$ denotes the logistic sigmoid function:

$$\sigma(z) = \frac{1}{1 + e^{-z}},$$

which maps real-valued inputs to the interval $(0, 1)$. The function $\tanh(\cdot)$ denotes the hyperbolic tangent function, which maps inputs to the interval $(-1, 1)$.

The proposed model extends this standard LSTM framework by introducing copula-based activation functions in the output layer to capture multivariate dependencies among the response variables.

The LSTM model is implemented with two stacked LSTM layers, each consisting of 64 units. Batch normalization is used to stabilize training, and dropout layers with a rate of 30% are included to prevent overfitting. The output layer consists of three response variables, each transformed using a copula-based activation function.

Trainable parameters for copula-based activations, such as θ_{Clayton} and θ_{Gumbel} , are learned during training, allowing the model to dynamically adapt to dependency structures. The models are evaluated using mean squared error (MSE), mean absolute error (MAE), log-likelihood for copula-based dependency estimation, and Shewhart control charts for stability assessment.

Multiple LSTM models are considered by varying the output activation function:

- LSTM with Clayton Copula Activation: Captures lower tail dependence.
- LSTM with Gumbel Copula Activation: Captures upper tail dependence.
- LSTM with Combined Clayton-Gumbel Activation: Models both left and right tail dependence.
- LSTM with ReLU Activation: Introduces non-linearity without dependency modeling.
- LSTM with Clayton-ReLU Activation: Combines dependency modeling with ReLU non-linearity.
- LSTM with Sigmoid Activation: Suitable for probabilistic or binary outputs.

LSTM networks, introduced by [1], address the vanishing gradient problem in standard recurrent neural networks by incorporating memory and gating mechanisms. While common activation functions such as ReLU and Sigmoid are effective for single-output tasks, they do not explicitly capture interdependencies between multiple response variables. This research integrates

copula-based activations to enhance the modeling of nonlinear and tail dependencies in multivariate responses, with applications in survival analysis, financial volatility modeling, and other time-dependent processes.

The hybrid CNN-LSTM architecture leverages the spatial feature extraction capability of CNNs and the sequential modeling ability of LSTMs, making it particularly effective for time series forecasting and multivariate prediction. While CNNs extract local patterns, LSTMs preserve long-range temporal dependencies. Standard activation functions do not capture multivariate dependencies; thus, copula-based activation functions are introduced in the output layer.

Let $X \in \mathbb{R}^{T \times d}$ be the input time series of length T with d features.

$$\begin{aligned} Z_t^{(1)} &= \text{ReLU} \left(\sum_{j=0}^{k-1} K_j^{(1)} X_{t-j} + b^{(1)} \right), \\ Z_{\text{pool},i}^{(1)} &= \max \left(Z_{2i}^{(1)}, Z_{2i+1}^{(1)} \right), \\ Z_t^{(2)} &= \text{ReLU} \left(\sum_{j=0}^{k-1} K_j^{(2)} Z_{\text{pool},t-j}^{(1)} + b^{(2)} \right), \\ Z_{\text{pool},i}^{(2)} &= \max \left(Z_{2i}^{(2)}, Z_{2i+1}^{(2)} \right), \end{aligned}$$

where $K^{(1)}, K^{(2)} \in \mathbb{R}^{k \times d}$ are the convolutional kernels and $b^{(1)}, b^{(2)} \in \mathbb{R}$ are biases.

The output from the convolutional layers is fed into a two-layer LSTM:

$$\begin{aligned} h_t^{(1)}, C_t^{(1)} &= \text{LSTM}^{(1)}(Z_{\text{pool},t}^{(2)}, h_{t-1}^{(1)}, C_{t-1}^{(1)}), \\ h_t^{(2)}, C_t^{(2)} &= \text{LSTM}^{(2)}(h_t^{(1)}, h_{t-1}^{(2)}, C_{t-1}^{(2)}), \end{aligned}$$

with recurrent dropout and batch normalization applied after each LSTM layer. The final output prediction is:

$$\hat{Y} = g_{\text{copula}} \left(W_{\text{out}} h_T^{(2)} + b_{\text{out}} \right),$$

where $W_{\text{out}} \in \mathbb{R}^{3 \times 64}$, $b_{\text{out}} \in \mathbb{R}^3$, and $g_{\text{copula}} : \mathbb{R}^3 \rightarrow \mathbb{R}^3$ is a multivariate copula-based activation function modeling dependencies across output components.

Copula parameters such as θ_{Clayton} (left-tail dependence) and θ_{Gumbel} (right-tail dependence) are optimized during training via gradient-based methods. Performance is evaluated using MSE, MAE, log-likelihood, and Shewhart control charts.

Variants of the CNN-LSTM model include:

- CNN-LSTM with Clayton Copula Activation

- CNN-LSTM with Gumbel Copula Activation
- CNN-LSTM with Combined Clayton-Gumbel Copula Activation
- CNN-LSTM with ReLU Activation
- CNN-LSTM with Clayton-ReLU Activation
- CNN-LSTM with Sigmoid Activation

By explicitly modeling complex interdependencies, the CNN-LSTM with copula activation is well-suited for multivariate prediction in domains such as survival analysis, finance, and healthcare.

3.3 Censoring Mechanisms in Survival Analysis

Censoring occurs when the true event time $T \in \mathbb{R}_+$ is only partially observed. The three common types are right, left, and interval censoring.

Right censoring: The event has not occurred by the censoring time $C \in \mathbb{R}_+$. The observed data are:

$$T^* = \min(T, C), \quad \delta = \mathbb{I}(T \leq C),$$

where T^* is the observed time and $\delta \in \{0, 1\}$ is the event indicator, with $\delta = 1$ indicating the event is observed. This type of censoring is handled by methods such as the Kaplan-Meier estimator [19], Cox proportional hazards model [18], and copula-based survival models [25, 26].

Left censoring: The event occurred before the observation began, but the exact time is unknown. This corresponds to observing $T^* \leq C$. Techniques for handling left-censored data include Turnbull’s estimator [27] and parametric models with upper-bound likelihood components [28].

Interval censoring: The event is known to have occurred within a time interval (L, R) , such that $T \in (L, R)$, but the exact time is unobserved. Suitable estimation methods include the nonparametric MLE [29], EM algorithms, and multiple imputation techniques [30].

Modern deep learning-based survival models such as DeepSurv [31] and DeepHit [32] are primarily designed for right-censored data, often leveraging the Cox partial likelihood or inverse probability of censoring weighted (IPCW) losses. Extending these models to handle left or interval censoring requires modified loss functions and appropriately structured likelihoods.

3.4 Rationale for Using CNN-LSTM with Learnable Copula in Survival Analysis

Survival analysis with high-dimensional, longitudinal, or irregularly spaced data demands models capable of learning both local and long-range temporal dependencies while capturing nonlinear inter-variable relationships. To this end, we propose a hybrid CNN-LSTM architecture augmented with a learnable copula layer. This architecture is designed to model dynamic survival processes under right censoring with complex covariate interactions.

Let $\mathbf{X} = (\mathbf{X}_1, \dots, \mathbf{X}_T) \in \mathbb{R}^{T \times d}$ denote a multivariate time series of d -dimensional covariates observed at T time steps. The CNN-LSTM architecture processes \mathbf{X} as follows:

- 1D convolutional layers extract local temporal patterns (e.g., abrupt shifts or warning signals in biomarkers).
- LSTM layers capture long-term dependencies and cumulative risk dynamics over time.
- Batch normalization and dropout layers are used for regularization and training stability.
- A final dense layer projects the learned representations to the output space (e.g., survival probabilities or hazards).
- A learnable copula activation function models dependencies between multiple predicted outcomes or risks.

While CNNs reduce parameter complexity and enhance local feature detection, LSTMs retain temporal memory, making them suitable for modeling censored survival trajectories. The addition of a learnable copula layer $C_\theta(\cdot)$, where θ denotes the copula parameter(s), allows for:

- **Modeling Tail Dependencies:** Capture asymmetric dependencies, such as those in clustered failure times or extreme risk profiles.
- **Decoupling Marginals and Dependence:** Allow separate learning of marginal distributions and their joint dependency structure.
- **Adaptivity:** Trainable parameters θ enable use of parametric (e.g., Clayton, Gumbel, Gaussian) or nonparametric copulas.
- **Multivariate Generalization:** Facilitate modeling of multiple risks, competing events, and longitudinal trajectories.

This hybrid design enhances the model’s ability to represent the survival distribution flexibly and accurately in the presence of censoring, high-dimensional covariates, and complex dependency structures.

3.5 Model Evaluation and Residual Analysis

We apply the Shewhart control chart to residuals-defined as the difference between actual and predicted survival times-to evaluate model performance. These charts are designed to systematically detect model drift and outliers, ensuring stability and reliability of predictions.

Residuals are computed as:

$$R = Y - \hat{Y},$$

where $Y \in \mathbb{R}_+$ denotes the observed (possibly censored) survival time, and $\hat{Y} \in \mathbb{R}_+$ is the predicted survival time from the model.

The Shewhart control chart identifies instability using control limits:

$$\text{UCL} = \bar{R} + 2\sigma_R, \quad \text{LCL} = \bar{R} - 2\sigma_R,$$

where \bar{R} is the mean residual across samples or simulation folds, and σ_R is the empirical standard deviation of residuals.

To quantify the chart’s sensitivity, the average run length (ARL) is computed:

$$\text{ARL} = \frac{1}{\mathbb{P}(\text{signal})},$$

where $\mathbb{P}(\text{signal})$ is the probability that a residual falls outside the control limits.

Models are evaluated across multiple simulations, and comparative performance is summarized under different copula-based activation functions.

Tracking out-of-control signals allows us to detect model degradation over time-particularly valuable in high-stakes domains such as healthcare-by identifying systematic errors in predictions and improving model trustworthiness.

While residual analysis measures pointwise prediction error, the ARL reflects how frequently the model signals a lack of stability. Together, they form a robust framework by integrating deep learning with traditional quality control methods.

Although Shewhart charts are traditionally used for continuous variables, their recent adaptations in machine learning enable monitoring of prediction drift and output variance. In our case, we apply control charts not to raw binary or categorical outcomes, but to smoothed probability residuals or posterior predictive summaries-making them continuous and suitable for such monitoring.

The ARL metric serves as a proxy for model consistency, reflecting the expected number of observations between instability signals. We compute ARL using posterior predictive residuals or log-likelihood trajectories over simulation replicates and cross-validation folds, enabling the detection of subtle changes in model calibration or dispersion [33].

We adopt 2σ control limits (rather than the traditional 3σ) to increase sensitivity to small or transient shifts-aligned with practices in early-warning systems and small-shift detection scenarios [34]. Finally, we emphasize that control charts and ARL metrics are complementary to standard survival model evaluation tools such as the Brier score, time-dependent AUC, and calibration plots. Their inclusion offers insights into temporal robustness and distributional stability, especially in the presence of censoring or simulation-driven variance [35]. While the application of control charts and ARL in survival analysis with categorical endpoints is non-traditional, our methodology-grounded in smoothing and posterior prediction-makes it both empirically valid and interpretively meaningful.

4 Simulation Study

To evaluate the performance of the proposed CNN-LSTM and LSTM models augmented with copula-based activation functions, we developed a comprehensive computational pipeline that simulates realistic survival analysis settings. The synthetic dataset was designed to reflect clinical scenarios in which individuals may experience multiple, potentially correlated, time-to-event outcomes. The data generation process incorporates both censored and uncensored survival times and produces heterogeneous response types-including continuous, binary, and categorical outcomes-thus enabling a robust evaluation of multi-task survival models under realistic conditions.

The simulation framework involves the generation of baseline survival times from Weibull distributions, the construction of dependent outcomes via additive noise mechanisms, and the introduction of right-censoring through exponential censoring distributions. Label transformations are subsequently applied to derive binary and ordinal categorical outputs from the continuous survival times, supporting multi-task prediction settings.

Additionally, we integrate differentiable copula activation layers-parameterized by either Clayton or Gumbel copulas-directly into the neural network architecture. These layers allow for dynamic, learnable modeling of inter-output dependencies via gradient-based optimization. The following outline the details of the simulation design and training methodology.

Step 1: Survival Time Generation. For each individual $i = 1, \dots, n$, we generated a baseline survival time T_{i1} from a Weibull distribution:

$$T_{i1} \sim \text{Weibull}(k = 1.5, \lambda = 2),$$

where k is the shape parameter and λ the scale parameter.

Step 2: Dependent Time-to-Event Variables. To simulate correlated survival outcomes, two additional responses T_{i2} and T_{i3} were constructed with strong linear dependence on T_{i1} plus additive noise:

$$\begin{aligned} T_{i2} &= \rho T_{i1} + (1 - \rho)\epsilon_{i2}, & \epsilon_{i2} &= W_{i2} + N_{i2}, & W_{i2} &\sim \text{Weibull}(k = 1.5, \lambda = 2), & N_{i2} &\sim \mathcal{N}(0, 0.5), \\ T_{i3} &= \rho T_{i1} + (1 - \rho)\epsilon_{i3}, & \epsilon_{i3} &= W_{i3} + N_{i3}, & W_{i3} &\sim \text{Weibull}(k = 1.5, \lambda = 2), & N_{i3} &\sim \mathcal{N}(0, 0.5), \end{aligned}$$

where $\rho = 0.9$ controls dependency strength.

Step 3: Right-Censoring Mechanism . Censoring times C_{ij} for $j = 1, 2, 3$ were independently generated from an exponential distribution,

$$C_{ij} \sim \text{Exponential}(\lambda = 0.1).$$

Then the observed survival outcomes were defined as observed survival times $T_{ij}^{(\text{obs})}$ and censoring status δ_{ij} for $j = 1, 2, 3$, as follows:

$$T_{ij}^{(\text{obs})} = \min(T_{ij}, C_{ij}) \text{ and } \delta_{ij} = I(T_{ij} \leq C_{ij}).$$

Step 4: Label Transformation. The observed survival times were further transformed to simulate different response types:

- Binary Response: $T_{i2}^{(\text{obs})}$ was binarized at threshold 5,

$$Y_{i2} = \mathbb{I}(T_{i2}^{(\text{obs})} > 5),$$

where $\mathbb{I}(\cdot)$ indicates values above 5, and 0 otherwise.

- Categorical Response: $T_{i3}^{(\text{obs})}$ was discretized into three ordinal categories, denoted by Y_{i3} :

$$\text{Low} = (0, 2], \quad \text{Medium} = (2, 5], \quad \text{High} = (5, \infty),$$

using the `cut()` function.

Copula activation functions offer a principled approach to modeling complex dependencies between output variables in deep learning architectures. In this study, we incorporate parametric copulas specifically the Clayton and Gumbel copulas as activation functions within our neural network. Crucially, the copula parameters are treated as learnable components, enabling the model to adaptively infer the strength and type of dependency from data during training.

Let U and V be two transformed marginal outputs (e.g., predicted probabilities or risks) such that $U, V \in [0, 1]$. The Clayton and Gumbel copulas are defined in Equation 1 and Equation 2, respectively.

Each copula function is parameterized by θ , which controls the strength of dependence. The Clayton copula captures lower tail dependence, whereas the Gumbel copula captures upper tail dependence.

Instead of fixing θ , we initialize it with sensible default values and allow it to be updated during training via backpropagation:

$$\theta_{\text{Clayton}} = 1.0, \quad \theta_{\text{Gumbel}} = 2.0. \quad (4)$$

The parameters in Equation 4 are then optimized jointly with other model parameters using gradient-based methods. Let \mathcal{L} denote the overall loss function (e.g., negative log-likelihood or cross-entropy). Gradients are computed with respect to θ :

$$\theta \leftarrow \theta - \eta \frac{\partial \mathcal{L}}{\partial \theta},$$

where η is the learning rate. To ensure that θ remains within the valid domain of the copula (e.g., $\theta > 0$), we apply a softplus transformation:

$$\theta = \log \left(1 + e^{\phi} \right),$$

where $\phi \in \mathbb{R}$ is the actual learnable parameter in the network.

Learning the copula parameter allows the model to dynamically adjust to the dependency structure inherent in the data, thereby improving flexibility and generalization. This approach is particularly useful in structured prediction tasks such as survival analysis, time series forecasting, or modeling of joint risks, where capturing tail dependencies is crucial for accurate predictions. Furthermore, the learned θ values provide interpretable insights into the nature of inter-variable dependence.

To clarify the simulation setup in our study: although we generate three response variables, our copula-based dependency modeling utilizes bivariate copulas, specifically Clayton and Gumbel copulas, applied to pairs of outputs. The three simulated outputs are:

- T_{i1} : a continuous time-to-event outcome,
- T_{i2} : a binary variable derived from thresholding T_{i1} ,
- T_{i3} : an ordinal categorical variable derived by discretizing T_{i1} .

While the simulation involves three variables, our neural network architecture applies copula activation functions at the pairwise level (e.g., between (T_{i1}, T_{i2}) , (T_{i1}, T_{i3}) , or (T_{i2}, T_{i3})). This approach is consistent with established practices in copula modeling, which often rely on bivariate constructions to manage complexity while capturing essential dependence structures [10, 11]. In our architecture, each output head generates a marginal prediction, such as survival probability or logit score. These predictions are then transformed into pseudo-observations in $[0, 1]$, and passed through a bivariate copula activation layer. The copula layer introduces dependency modeling via a differentiable transformation with a learnable parameter θ . This parameter is optimized jointly with network weights using backpropagation, allowing the model to infer dependencies directly from data during training.

For multiple output tasks, we incorporate one or more pairwise copula transformations, depending on the specific experimental configuration. This strategy provides interpretability and modularity, while remaining computationally tractable. As a future extension, we intend to explore multivariate constructions such as vine copulas [23, 24] for more comprehensive modeling of higher-order dependencies across all outputs.

From the LSTM and CNN-LSTM models based on residual Shewhart control charts in Figure 1 and Figure 2, we notice that the CNN-LSTM models with Copula-based activations outperformed LSTM models with copula-based activations in terms of residual variability and the frequency of outliers in Response_1, Response_2, and Response_3. However, both CNN-LSTM and LSTM models with ReLU and Sigmoid activations exhibited instability in the binary variable Y_2 and categorical variable Y_3 . Notably, CNN-LSTM with Clayton-ReLU activation improved residual stability, reducing extreme shifts in the control chart in Y_2 and Y_3 . Our findings suggest that hybrid copula-based Clayton-ReLU activation mitigates instability issues more effectively than models using ReLU or Sigmoid activations for binary variable Response_2 and categorical variable Response_3. Based on this simulation study, we recommend the CNN-LSTM model with Clayton-ReLU activation for analyzing multivariate response data, including continuous, binary, and categorical variables.

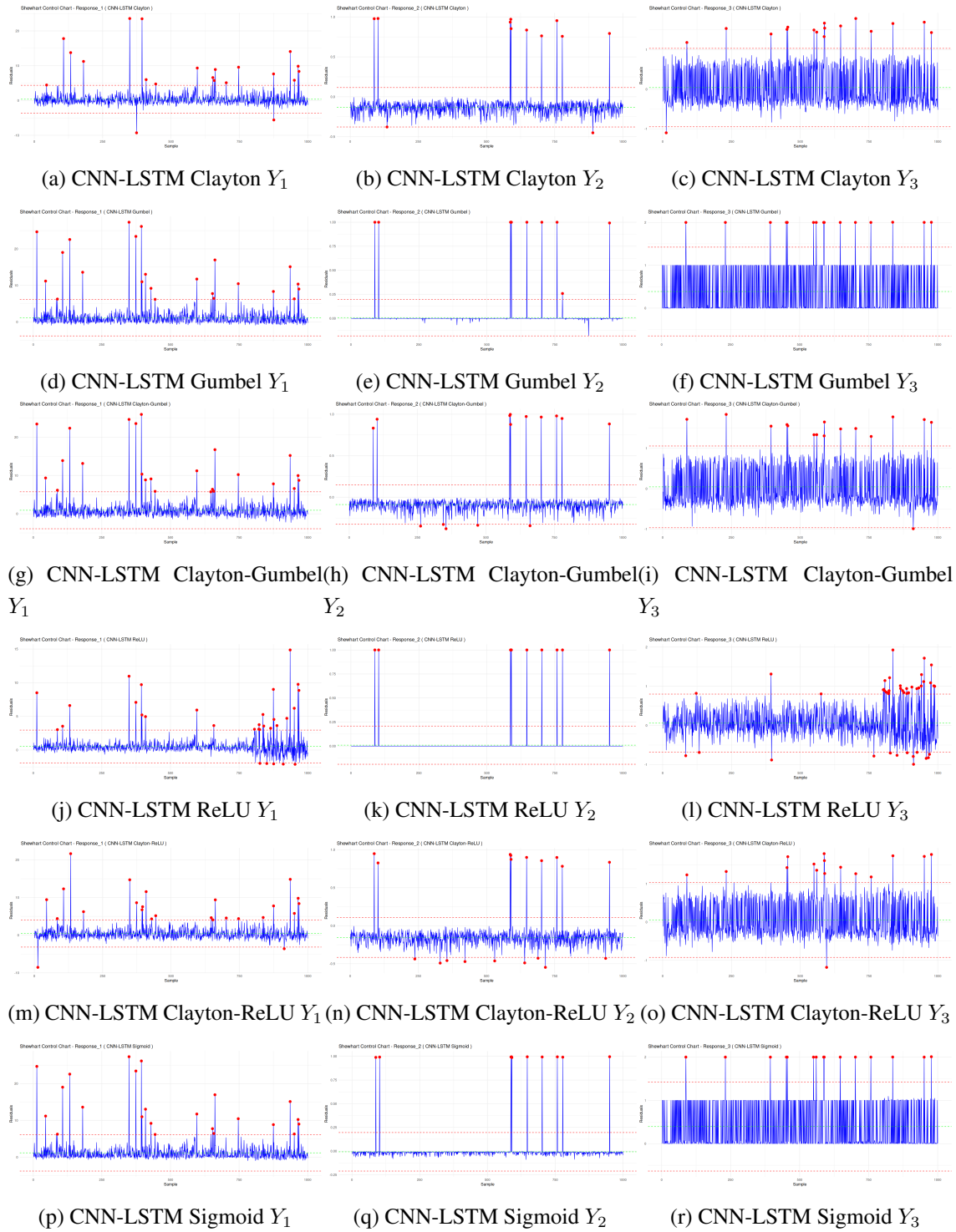


Figure 1: Residual Shewhart Control Charts of CNN-LSTM Models with Simulated Data.

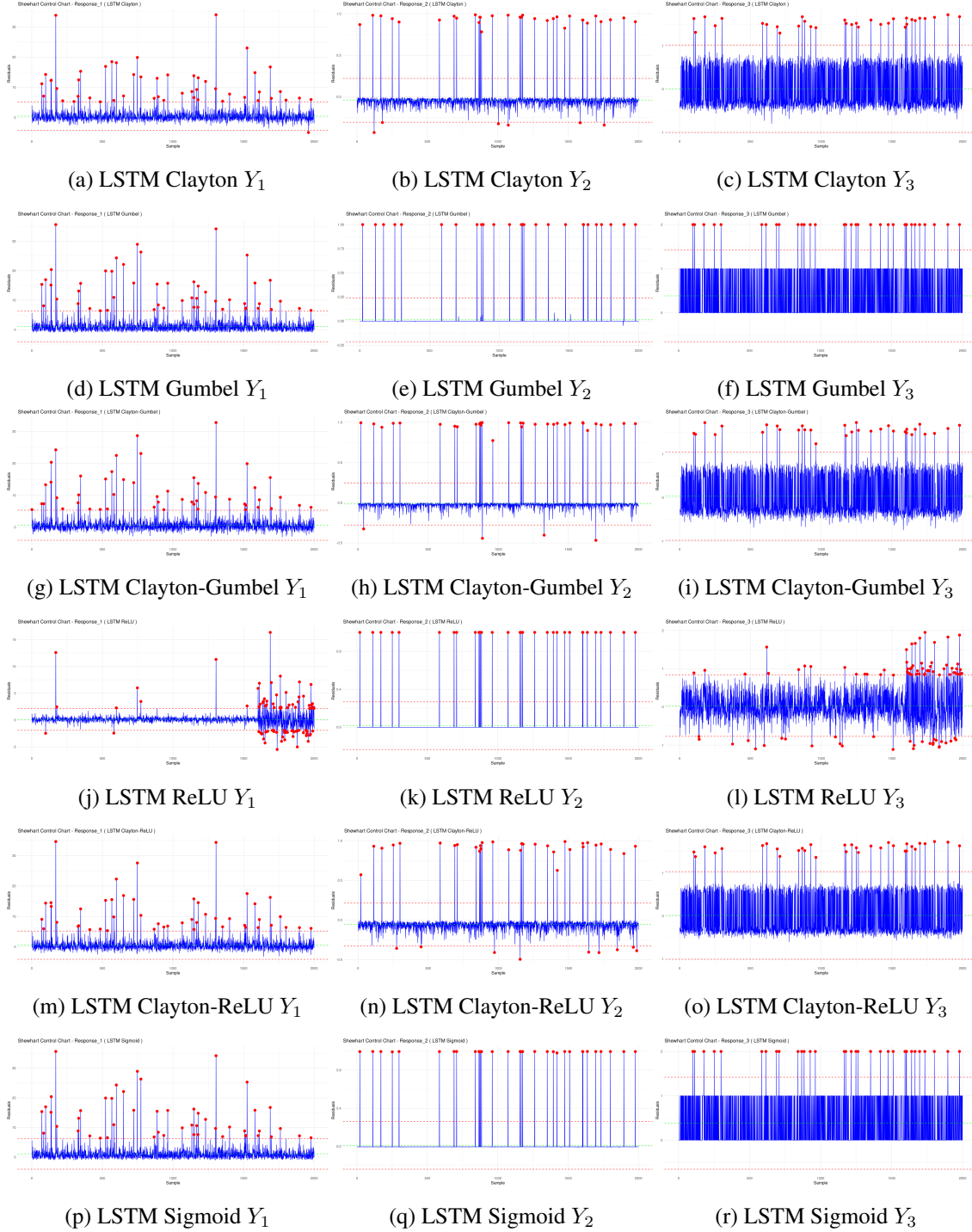


Figure 2: Residual Shewhart Control Charts of LSTM Models with Simulated Data.

Table 1: Model Comparison with Simulated Data.

Model	Response	Mean_Residual	SD_Residual	Mean_ARL	SD_ARL
CNN-LSTM Clayton	Response_1	0.3674	2.0058	46.0952	16.8473
CNN-LSTM Clayton	Response_2	-0.1311	0.1234	79.2500	16.8473
CNN-LSTM Clayton	Response_3	0.0427	0.4955	57.4706	16.8473
CNN-LSTM Gumbel	Response_1	1.1632	2.4861	42.0870	26.8608
CNN-LSTM Gumbel	Response_2	0.0081	0.0951	95.1000	26.8608
CNN-LSTM Gumbel	Response_3	0.3886	0.5174	61.0625	26.8608
CNN-LSTM Clayton-Gumbel	Response_1	0.9159	2.4122	40.3333	12.6967
CNN-LSTM Clayton-Gumbel	Response_2	-0.0880	0.1188	63.4000	12.6967
CNN-LSTM Clayton-Gumbel	Response_3	0.0456	0.5057	61.0625	12.6967
CNN-LSTM ReLU	Response_1	0.5227	1.2212	31.2258	39.8169
CNN-LSTM ReLU	Response_2	0.0100	0.0995	95.1000	39.8169
CNN-LSTM ReLU	Response_3	0.0585	0.3712	21.9778	39.8169
CNN-LSTM Clayton-ReLU	Response_1	0.4347	1.7965	38.7200	11.1716
CNN-LSTM Clayton-ReLU	Response_2	-0.1551	0.1303	50.0526	11.1716
CNN-LSTM Clayton-ReLU	Response_3	0.0562	0.4892	61.0625	11.1716
CNN-LSTM Sigmoid	Response_1	1.2055	2.4707	42.0870	26.8608
CNN-LSTM Sigmoid	Response_2	-0.0071	0.1015	95.1000	26.8608
CNN-LSTM Sigmoid	Response_3	0.3958	0.5141	61.0625	26.8608
LSTM Clayton	Response_1	0.4908	2.3292	38.7843	10.6910
LSTM Clayton	Response_2	-0.0414	0.1321	52.0526	10.6910
LSTM Clayton	Response_3	0.0093	0.5065	59.9394	10.6910
LSTM Gumbel	Response_1	1.1114	2.5938	39.5600	18.2995
LSTM Gumbel	Response_2	0.0131	0.1133	76.0769	18.2995
LSTM Gumbel	Response_3	0.3825	0.5190	59.9394	18.2995
LSTM Clayton-Gumbel	Response_1	0.6306	2.3563	38.7843	11.0577
LSTM Clayton-Gumbel	Response_2	-0.0153	0.1307	54.9444	11.0577
LSTM Clayton-Gumbel	Response_3	0.0337	0.5074	59.9394	11.0577
LSTM ReLU	Response_1	0.1190	1.0148	24.0843	22.2052
LSTM ReLU	Response_2	0.0160	0.1255	61.8125	22.2052
LSTM ReLU	Response_3	0.0316	0.4009	22.6591	22.2052
LSTM Clayton-ReLU	Response_1	0.5436	2.3281	41.2083	9.4445
LSTM Clayton-ReLU	Response_2	-0.0573	0.1350	48.4634	9.4445
LSTM Clayton-ReLU	Response_3	0.0138	0.5107	59.9394	9.4445
LSTM Sigmoid	Response_1	1.1114	2.5938	39.5600	12.3424
LSTM Sigmoid	Response_2	0.0112	0.1254	61.8125	12.3424
LSTM Sigmoid	Response_3	0.3826	0.5190	59.9394	12.3424

Table 1 presents a comparison of CNN-LSTM and LSTM models using different activation functions and copula methods for three response variables. The evaluation is based on four key metrics: mean residual, standard deviation of residuals, mean ARL, and standard deviation of ARL. The mean residual represents the average difference between predicted and actual values, while the standard deviation of residuals indicates the variability in prediction errors. Mean ARL measures how often the model detects changes, with higher values indicating fewer false alarms. The standard deviation of ARL reflects the consistency of change detection.

Figure3 summarizing mean ARL values from Table 1 across different models and response types. This visualization helps compare how each model performs across Response_1, Response_2, and Response_3 in terms of ARL. In addition, there are two additional bar graphs for Mean Residual by Model and Response and Standard Deviation of Residuals by Model and Response in Figure3. Mean Residual by Model and Response highlights the average error for each model across the three response variables. Standard Deviation of Residuals by Model and Response indicates the spread or variability of the residuals for each model and response. CNN-LSTM Gumbel and CNN-LSTM Sigmoid exhibit particularly high residuals for Response_1, exceeding 1.1, which indicates challenges in capturing this response accurately. For Response_2, CNN-LSTM Clayton-ReLU and CNN-LSTM Clayton show the lowest residual bias, with values of -0.1551 and -0.1311, respectively. The standard deviation of residuals remains relatively small, ranging between 0.1 and 0.13, reflecting stable predictions across models. The lowest bias for Response_3 is observed in CNN-LSTM Clayton-Gumbel and LSTM Clayton, with values of 0.0456 and 0.0093, respectively. The standard deviation of residuals remains below 0.52, indicating consistent performance across copula methods.

A higher mean ARL suggests that a model detects fewer false alarms. CNN-LSTM ReLU and CNN-LSTM Sigmoid achieve the highest mean ARL values for Response_2, both at 95.1, indicating strong stability. However, as shown in Figure 1 and Figure 2, both CNN-LSTM and LSTM models with ReLU and Sigmoid activations exhibit instability in the binary variable Response_2 and categorical variable Response_3. Therefore, we conclude that the mean ARL values for Response_2 with CNN-LSTM ReLU and CNN-LSTM Sigmoid may not be trustworthy. In contrast, LSTM ReLU has the lowest mean ARL for Response_1 at 24.08, indicating it reacts more quickly to changes. This is consistent with its stability in the residual Shewhart chart in Figure 2. The ReLU activation enhances model stability, particularly for CNN-LSTM models for Response_1. Clayton-ReLU Copulas reduce residuals, making them suitable choices for Response_2.

Overall, CNN-LSTM captures complex dependencies more effectively but exhibits higher

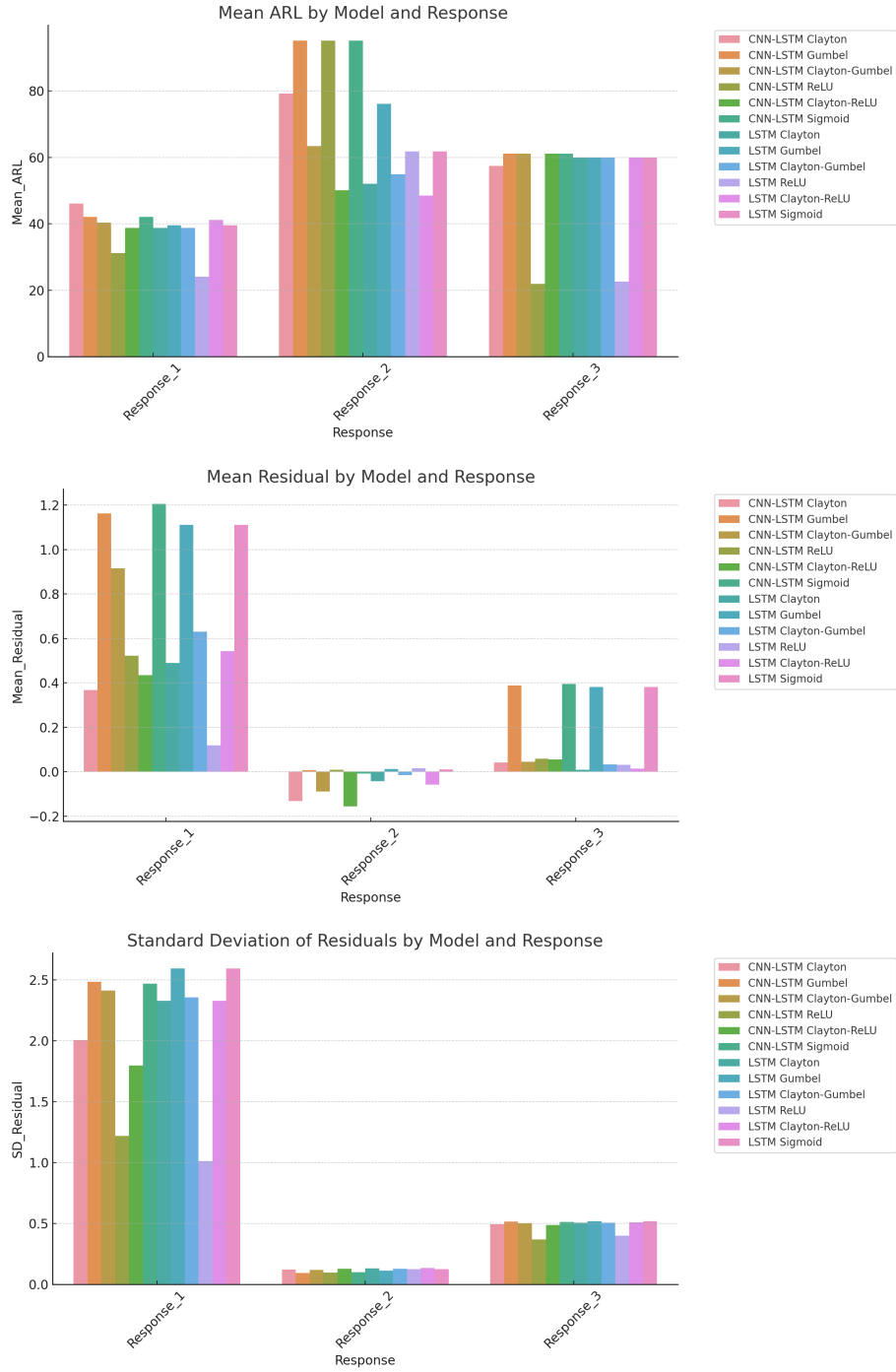


Figure 3: Mean ARL, Mean Residual and Standard Deviation of Residuals by Model and Response with Simulated Data.

residual fluctuations, particularly for Response_1. LSTM models provide more stable predictions with lower residual variance. For Response_2 and Response_3, Clayton-ReLU activation functions yield the most stable performance.

5 Breast Cancer Real Data Analysis

Breast Cancer Gene Expression Profiles (METABRIC), likely includes gene expression data related to breast cancer, where each sample corresponds to a breast cancer patient, and the features represent the expression levels of various genes. It likely contains a variety of columns with features such as: Gene expression levels: These are numerical values representing the expression levels of different genes in each patient. Patient metadata: Includes attributes like age, tumor stage, survival status, etc. Event time and censoring information: For survival analysis, you might have columns for the time until the event (e.g., death or recurrence) and a censoring indicator (1 = event occurred, 0 = censored). With this data, we can predict survival times using the gene expression data and clinical features, classify patients into different groups (e.g., tumor stage, survival status), identify genes whose expression levels differ significantly between different subgroups (e.g., cancerous vs. normal), and investigate the relationship between gene expression levels and responses to specific cancer treatments. In this research, we use the METABRIC (Molecular Taxonomy of Breast Cancer International Consortium) dataset, which contains clinical and genomic data for breast cancer patients. The preprocessing pipeline is designed to prepare the data for survival analysis, where the goal is to predict patient survival time and event status (death or censored) using clinical features and gene expression data. We downloaded the METABRIC dataset from the Kaggle website. The dataset contains both clinical variables (e.g., survival times, tumor stage) and genomic features (e.g., gene expression levels). The file path to the dataset must be specified, and once loaded, the dataset is examined to understand its structure, including the names of the columns.

Table 2 provides a detailed summary of six key variables extracted from the METABRIC (Molecular Taxonomy of Breast Cancer International Consortium) dataset. The dataset comprises information for 1,310 patients, with no missing values for any of the selected variables. The statistics presented include measures of central tendency and variability for numeric variables, and frequency distributions for categorical variables.

The variable `survival_time` captures the follow-up time (in months) until either death or censoring. The average survival time is 127.7 months, with a standard deviation of 78.5 months, indicating substantial variability in patient outcomes. The median survival is 117.7 months, which

Table 2: METABRIC Data Summary Statistics

No	Variable	Stats / Values	Freqs (% of Valid)	Valid	Missing
1	survival_time [numeric]	Mean (sd): 127.7 (78.5) Min = Med = Max: 0.1 = 117.7 = 351 IQR (CV): 128.1 (0.6) 1199 distinct values	–	1310 (100.0%)	0 (0.0%)
2	event_status [numeric]	1 distinct value	0: 1310 (100.0%)	1310 (100.0%)	0 (0.0%)
3	age [numeric]	Mean (sd): 60.3 (13) Min = Med = Max: 21.9 = 61 = 96.3 IQR (CV): 19 (0.2) 1141 distinct values	–	1310 (100.0%)	0 (0.0%)
4	tumor_stage [numeric]	Mean (sd): 1.8 (0.6) Min = Med = Max: 1 = 2 = 4 IQR (CV): 1 (0.4)	1: 442 (33.7%) 2: 752 (57.4%) 3: 108 (8.2%) 4: 8 (0.6%)	1310 (100.0%)	0 (0.0%)
5	er_status [character]	1. Negative 2. Positive	Negative: 303 (23.1%) Positive: 1007 (76.9%)	1310 (100.0%)	0 (0.0%)
6	her2_status [character]	1. Negative 2. Positive	Negative: 1149 (87.7%) Positive: 161 (12.3%)	1310 (100.0%)	0 (0.0%)

closely approximates the interquartile range (IQR) of 128.1 months, suggesting a right-skewed distribution. The minimum and maximum observed survival times are 0.1 and 351 months, respectively. The coefficient of variation (CV), a standardized measure of dispersion, is 0.6, and there are 1,199 unique values, demonstrating a high level of granularity in this continuous variable.

The `event_status` variable is coded numerically, though only one distinct value (0) appears in this subset, indicating that all patients in this subset were censored and no events (deaths) were recorded. All 1,310 entries are valid, with no missing data. This suggests either a data coding issue or that the sample was filtered to include only censored individuals.

The `age` variable captures the patient’s age at diagnosis. The average age is 60.3 years, with a standard deviation of 13 years. The observed ages range from 21.9 to 96.3 years, with a median of 61 years and an IQR of 19 years. The CV is 0.2, indicating low relative variability. There are 1,141 unique age values, suggesting minimal rounding or grouping of age measurements.

The `tumor_stage` variable is a numeric representation of disease progression, ranging from stage 1 to 4. The mean stage is 1.8, with a standard deviation of 0.6, and the median stage is 2. The IQR is 1, and the CV is 0.4, pointing to moderate dispersion. The distribution across tumor stages is as follows:

- Stage 1: 442 patients (33.7%)
- Stage 2: 752 patients (57.4%)

- Stage 3: 108 patients (8.2%)
- Stage 4: 8 patients (0.6%)

This indicates that the majority of patients were diagnosed at early stages, particularly stage 2.

The `er_status` is a binary categorical variable indicating the presence (Positive) or absence (Negative) of estrogen receptors in tumor cells. Among the 1,310 patients:

- Positive ER status: 1,007 patients (76.9%)
- Negative ER status: 303 patients (23.1%)

This shows that the majority of tumors were ER-positive, which is clinically significant for treatment decisions involving hormone therapy.

Similarly, `her2_status` categorizes the presence of human epidermal growth factor receptor 2 (HER2). The distribution is as follows:

- Negative HER2 status: 1,149 patients (87.7%)
- Positive HER2 status: 161 patients (12.3%)

HER2-positive tumors often require different therapeutic strategies, such as targeted therapies like trastuzumab.

The METABRIC dataset, as summarized in Table 2 is comprehensive and clean, with no missing data across the selected variables. The dataset exhibits rich variability in continuous measures such as survival time and age, and includes clinically relevant categorical variables such as ER and HER2 status. This robust data foundation supports rigorous modeling and inferential analysis in the context of breast cancer prognosis and treatment stratification.

To improve clarity and consistency, the columns of the dataset are renamed with more descriptive names. Specifically, the survival time column, `overall_survival_months`, is renamed to `survival_time`, and the event status column, `overall_survival`, is renamed to `event_status`. Additional columns such as `age_at_diagnosis`, `tumor_stage`, `er_status`, and `her2_status` are also renamed for clarity.

The `event_status` column, which originally contains categorical values (such as “Dead” or “Alive”), is converted into a binary format. This transformation allows the survival analysis model to treat the event status as a binary outcome, where 1 indicates that the patient has died (event occurred), and 0 indicates that the patient is either alive or the data is censored (event not observed).

The dataset may contain missing values for some columns. To ensure that only complete cases are used for analysis, any rows with missing data are removed from the dataset. This step is necessary to ensure the integrity of the data, as missing values can introduce biases or errors in survival models.

Several key parameters are defined for the model: The 'timesteps' parameter defines the number of time steps for the model and is set to a fixed value of 10 in this study. It can be adjusted based on the specific requirements of the analysis. The number of features corresponds to the number of columns in the dataset that represent clinical or genomic variables (e.g., gene expression measurements). This includes both the clinical features and any other variables relevant to the survival analysis. The number of samples refers to the number of rows in the dataset, where each row represents an individual patient.

To feed the data into CNN-LSTM and LSTM models, which require three-dimensional input, the dataset is reshaped into a 3D array with dimensions representing (samples, time steps, features). This transformation ensures that the LSTM model can handle sequential data appropriately. In practice, this reshaped data would be replaced with actual gene expression data or other time-series features if available, rather than random values used for illustration.

The input data is normalized to have zero mean and unit variance. Normalization is an important step when working with deep learning models, as it helps the model converge faster and avoids issues caused by variables with different scales. This step ensures that the features are standardized, making the model more efficient and stable during training.

After normalization, the data is reshaped again to ensure that it is in the correct format for input into the LSTM model. The reshaped data maintains the dimensions required by the model, ensuring compatibility with the network architecture.

The output labels, which include the survival time and event status, are selected from the dataset. These labels represent the target variables for the survival model. The `survival_time` (`Response_1`) is a continuous variable representing the time until the event or censoring, while the `event_status` (`Response_2`) is a binary variable indicating whether the event (death) occurred. These labels are then converted into a matrix format to be fed into the model during training.

The preprocessing steps described above transform the METABRIC dataset into a structured and ready-to-use format for survival analysis. The dataset undergoes cleaning, renaming, normalization, and reshaping to prepare it for deep learning models, particularly LSTM networks. These steps ensure that the model receives appropriately formatted and normalized data for predicting survival outcomes, which will help in understanding patient prognosis and improving clinical

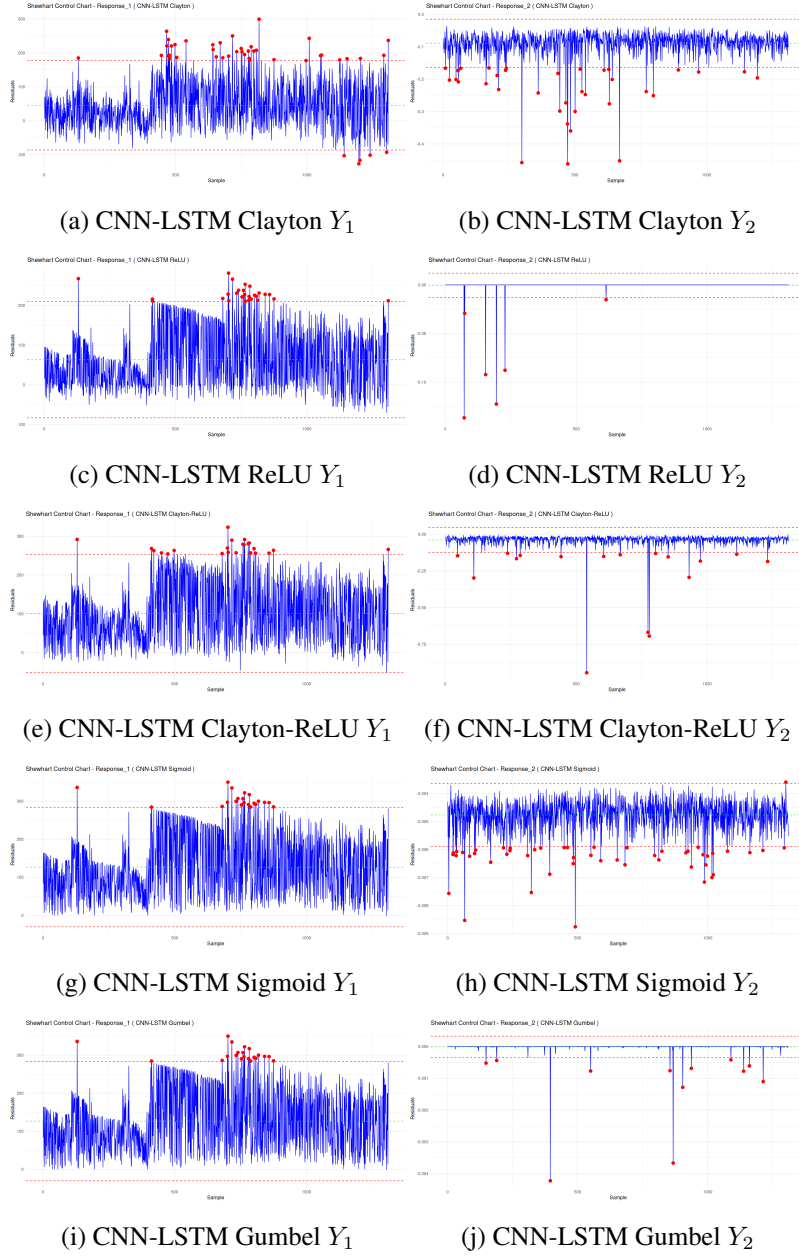


Figure 4: Residual Shewhart Control Charts of CNN-LSTM Models with METABRIC Data.

Table 3: Model Comparison with METABRIC Data.

Model	Response	Mean_Residual	SD_Residual	Mean_ARL	SD_ARL
CNN-LSTM Clayton	Response_1	45.50912	65.87903	29.11111	3.51758
CNN-LSTM Clayton	Response_2	-0.08897	0.03711	34.08571	3.51758
CNN-LSTM ReLU	Response_1	63.42113	73.22987	48.51852	38.05282
CNN-LSTM ReLU	Response_2	-0.00037	0.00623	102.33333	38.05282
CNN-LSTM Clayton-ReLU	Response_1	100.82850	76.27779	56.95652	10.92851
CNN-LSTM Clayton-ReLU	Response_2	-0.03900	0.04333	72.41176	10.92851
CNN-LSTM Sigmoid	Response_1	126.72640	78.47299	41.66667	11.07801
CNN-LSTM Sigmoid	Response_2	-0.00477	0.00056	26.00000	11.07801
CNN-LSTM Gumbel	Response_1	126.72640	78.47300	41.66667	42.01393
CNN-LSTM Gumbel	Response_2	-0.00001	0.00017	101.08333	42.01393
LSTM Clayton	Response_1	123.79849	77.40638	59.54545	25.27585
LSTM Clayton	Response_2	-0.36971	0.14856	23.80000	25.27585
LSTM ReLU	Response_1	58.5456	78.3978	41.6667	NA
LSTM ReLU	Response_2	0	0	NA	NA
LSTM Clayton-ReLU	Response_1	123.6547	77.2923	59.5455	24.8009
LSTM Clayton-ReLU	Response_2	-0.3768	0.1351	24.4717	24.8009
LSTM Sigmoid	Response_1	126.7264	78.4730	41.6667	9.6795
LSTM Sigmoid	Response_2	-0.0038	0.0011	27.9778	9.6795
LSTM Gumbel	Response_1	126.7264	78.4730	41.6667	121.6224
LSTM Gumbel	Response_2	-0.0002	0.0030	213.6667	121.6224

decision-making in breast cancer research.

From Figures 4 and 5, the residual Shewhart control charts illustrate differing stability levels across the CNN-LSTM and LSTM models. The CNN-LSTM and LSTM models with the Clayton-ReLU activation function demonstrate superior stability in the residuals for the binary variable Response_2, while the CNN-LSTM and LSTM models with ReLU, Sigmoid, and Gumbel activation functions exhibit instability, particularly in Response_2. We can conclude that the CNN-LSTM model with Clayton-based activation functions performs moderately well in controlling residual fluctuations.

Table 3 presents a comparison of CNN-LSTM and LSTM models for breast cancer data using different activation functions and copula-based dependency structures. The models are evaluated

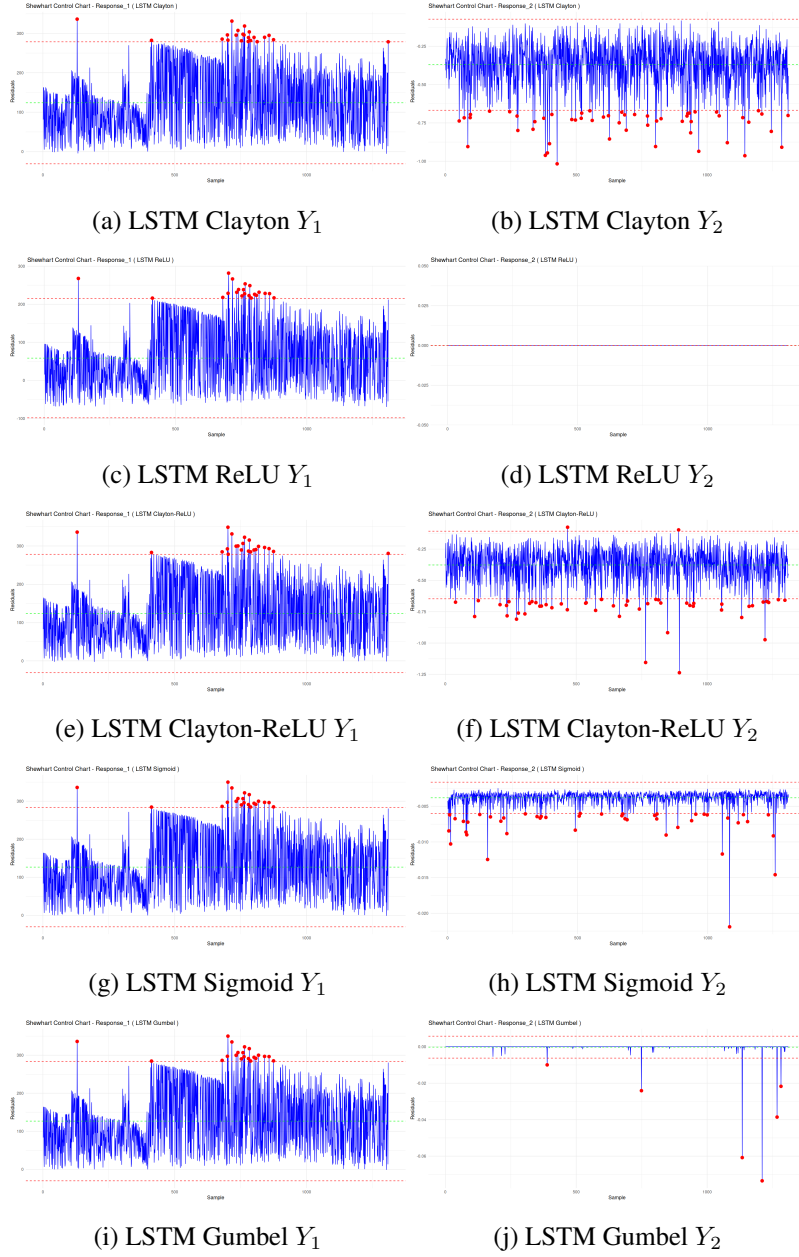


Figure 5: Residual Shewhart Control Charts of LSTM Models with METABRIC Data.

based on four key metrics: mean residual, standard deviation of residuals, mean ARL, and standard deviation of ARL. A lower mean residual indicates better prediction accuracy, while a lower standard deviation of residuals suggests more consistent predictions. A higher mean ARL means fewer false alarms, and a lower standard deviation of ARL indicates greater stability.

CNN-LSTM Clayton and CNN-LSTM ReLU exhibit moderate mean and standard deviation residuals, with values of (45.51, 65.87) and (63.42, 73.22), respectively. CNN-LSTM Sigmoid and CNN-LSTM Gumbel show the highest residuals at (126.73, 78.47), indicating poor prediction accuracy for Response_1. LSTM models also exhibit high residuals for Response_1, with LSTM Clayton-ReLU at (123.65, 77.29) and LSTM Gumbel at (126.73, 78.47), showing similar trends to CNN-LSTM. Models using ReLU activation, both CNN-LSTM and LSTM, have lower residuals than those using Sigmoid and Gumbel, making them more stable.

For Response_2, both CNN-LSTM and LSTM models generally perform well, with mean residuals close to zero because the residual Schwhart control charts does not work well in Figures 4 and 5. CNN-LSTM Clayton and CNN-LSTM Clayton-ReLU have small residual values of (-0.08897, 0.03711) and (-0.03900, 0.04333), making them reliable choices for stability. LSTM Gumbel and CNN-LSTM Gumbel display exceptionally low residuals at (-0.0002, 0.0030) and (-0.00001, 0.00017), respectively, indicating strong predictive performance because the residual Schwhart control charts does not work well in Figures 4 and 5.

In terms of detecting changes, CNN-LSTM ReLU and CNN-LSTM Gumbel achieve the highest mean ARL values for Response_2, at 102.33 and 101.08, suggesting they are less likely to trigger false alarms. CNN-LSTM Clayton, on the other hand, has lower ARL values for Y_2 , meaning it responds more frequently to changes.

Activation functions play a critical role in model performance. Sigmoid activation results in higher residuals for Y_1 , making it less suitable for high-variance data. Clayton Copula improves Y_2 predictions.

Overall, CNN-LSTM models tend to have greater residual fluctuations than LSTM models, particularly for Response_1. Sigmoid and Gumbel activations lead to higher instability in Response_1, making them less suitable for modeling this response.

Figure 6 summarizes mean residuals and mean ARL by model and response with METABRIC Data. Mean residuals by model and response shows how each model performs in terms of mean residuals for Response_1 and Response_2. The mean ARLs by model and response highlight how the models differ in their ARLs.

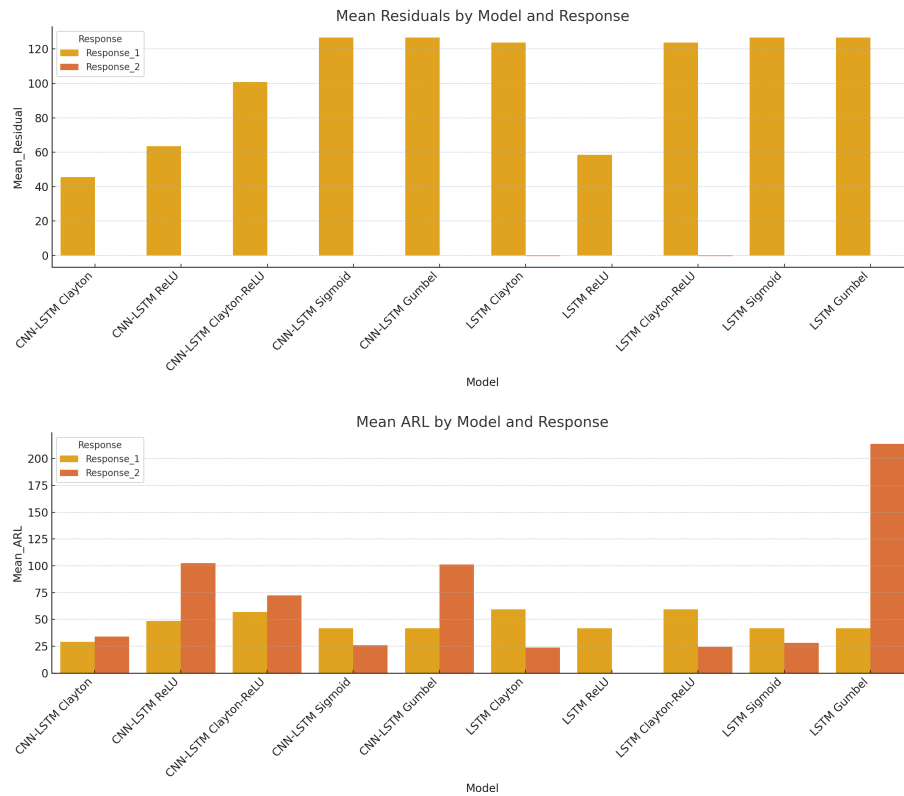


Figure 6: Mean Residuals and Mean ARL by Model and Response with METABRIC Data.

6 Conclusion

In this research, we introduce copula-based activation functions within CNN-LSTM survival analysis, demonstrating their effectiveness in modeling complex dependencies in failure time data. This work pioneers a hybrid framework that seamlessly integrates deep learning, copula theory, and quality control methods, providing accurate predictions while enhancing model reliability, interpretability, and robustness for real-world applications. Our proposed method effectively handles highly correlated, right-censored, multivariate survival response data.

In conclusion, our framework overcomes the challenges posed by censored data, captures intricate time dependencies, and models dependency structures using copulas, offering distinct advantages over traditional survival models. This approach holds significant potential in fields such as medical research, reliability engineering, and financial risk modeling, where precise survival predictions and robust handling of censored data are essential. Our future work will focus on competing-risks modeling for clustered survival data, further extending the CNN-LSTM framework with copula-based activation functions.

Acknowledgment

This work was supported by the National Research Foundation of Korea (NRF) grant funded by the Korea government(MSIT) (No. NRF-2021R1G1A1094116 and No. RS-2023-00240794). We thank the two respected referees, Associated Editor and Editor for constructive and helpful suggestions which led to substantial improvement in the revised version. For the sake of transparency and reproducibility, the R code for this study can be found in the following GitHub repository: R code GitHub site.

References

- [1] Hochreiter, S., and Schmidhuber, J. (1997). Long short-term memory. *Neural Computation*, **9**(8), 1735-1780. <https://doi.org/10.1162/neco.1997.9.8.1735>
- [2] LeCun, Y., Bottou, L., Bengio, Y. and Haffner, P. (1998). Gradient-based learning applied to document recognition. *Proceedings of the IEEE*, **86**(11), 2278-2324. <https://ieeexplore.ieee.org/document/726791>.

- [3] Harrell Jr, F. E., Lee, K. L., and Mark, D. B. (1996). Multivariable prognostic models: issues in developing models, evaluating assumptions and adequacy, and measuring and reducing errors. *Statistics in Medicine*, **15**, 361-387.
- [4] Calhoun, P., Su X., Nunn M., Fan J. (2018). Constructing multivariate survival trees: The MST package for R. *Journal of Statistical Software*, **83**, 1-21.
- [5] Hougaard, P (2000) *Analysis of multivariate survival data*. Springer, New York.
- [6] Nair, V. and Hinton, G. E. (2010). Rectified Linear Units Improve Restricted Boltzmann Machines. *In Proceedings of the 27th International Conference on Machine Learning (ICML 2010)*, 807-814.
- [7] Hinton, G. E. and Salakhutdinov, R. R. (2006). Reducing the Dimensionality of Data with Neural Networks. *Science*, **313(5786)**, 504-507.
- [8] Bishop, C. M. (2024). *Deep learning: Foundations and concepts*, Springer.
- [9] Kvamme, H., Borgan, I. and Scheel, I. (2019). Time-to-event prediction with neural networks and Cox Regression. *Journal of Machine Learning Research*, **20**, 1-30.
- [10] Joe, H. (1997). *Multivariate models and dependence concepts*. New York: Chapman and Hall.
- [11] Nelsen, R. B. (2013). *An introduction to copulas*. Springer Science & Business Media, 2nd.
- [12] Escarela, G. and Carriere, J. F. (2003). Fitting competing risks with an assumed copula. *Statistical Methods in Medical Research*, **12**, 333-349.
- [13] Emura, T. and Chen, Y.H. (2018). *Analysis of survival data with dependent censoring: copula-based approaches*. Springer.
- [14] Kwon, S, Ha, ID, Shih, J-H and Emura, T. (2022). Flexible parametric copula modeling approaches for clustered survival data. *Pharmaceutical Statistics*, **21**, 69-88.
- [15] Huang, X. and Zhang, N. (2008). Regression survival analysis with an assumed copula for dependent censoring: a sensitivity analysis approach. *Biometrics*, **64**, 1090-1099.
- [16] Kwon, J., Emura, T. and Ha, I.D. (2025) Copula-based deep neural networks for clustered survival data. *Communications for Statistical Applications and Methods*, **32**, 389-400.

- [17] Montgomery, D.C. (2007). Introduction to statistical quality control. Hoboken, NJ: John Wiley & Sons.
- [18] Cox, D. R. (1972). Regression models and life-tables. *Journal of the Royal Statistical Society. Series B (Methodological)*, **34(2)**, 187-220.
- [19] Kaplan, E. L., & Meier, P. (1958). Nonparametric estimation from incomplete observations. *Journal of the American Statistical Association*, **53(282)**, 457-481.
- [20] Ishwaran, H., Kogalur, U. B., Blackstone, E. H. and Lauer, M. S. (2008). Random survival forests. *The Annals of Applied Statistics*, **2(3)**, 841-860.
- [21] Binder, H. and Schumacher, M. (2008). Allowing for mandatory covariates in boosting estimation of sparse high-dimensional survival models. *BMC Bioinformatics*, **9(1)**, 14.
- [22] Van Belle, V., Pelckmans, K., Van Huffel, S., and Suykens, J. A.K. (2011). Support vector methods for survival analysis: a comparison between ranking and regression approaches. *Artificial Intelligence in Medicine*, **53(2)**, 107-118.
- [23] Aas, K., Czado, C., Frigessi, A., & Bakken, H. (2009). Pair-copula constructions of multiple dependence. *Insurance: Mathematics and Economics*, **44(2)**, 182–198.
- [24] Joe, H. (2014). *Dependence Modeling with Copulas*. CRC Press.
- [25] Oakes, D. (1989). Bivariate survival models induced by frailties. *Journal of the American Statistical Association*, **84(406)**, 487-493.
- [26] Shih, J. H., & Louis, T. A. (1995). Inference on the association parameter in copula models for bivariate survival data. *Biometrics*, **51(4)**, 1384-1399.
- [27] Turnbull, B. W. (1976). The empirical distribution function with arbitrarily grouped, censored and truncated data.
- [28] Sun, J. (2006). *The Statistical Analysis of Interval-Censored Failure Time Data*. Springer. *Journal of the Royal Statistical Society: Series B*, **38(3)**, 290-295.
- [29] Wellner, J. A., & Zhan, Y. (1997). A hybrid algorithm for computation of the nonparametric maximum likelihood estimator from censored data. *Journal of the American Statistical Association*, **92(439)**, 945-959.

- [30] De Gruttola, V., & Lagakos, S. W. (1989). Analysis of doubly-censored survival data, with application to AIDS. *Biometrics*, **45**(1), 1-11.
- [31] Katzman, J., Shaham, U., Cloninger, A., Bates, J., Jiang, T., & Kluger, Y. (2018). DeepSurv: Personalized treatment recommender system using a Cox proportional hazards deep neural network. *BMC Medical Research Methodology*, **18**(24).
- [32] Lee, C., Zame, W., Yoon, J., & van der Schaar, M. (2018). DeepHit: A deep learning approach to survival analysis with competing risks. In **Proceedings of the AAAI Conference on Artificial Intelligence**, 32(1).
- [33] Woodall, W. H. (2006). The use of control charts in health-care and public-health surveillance. *Journal of Quality Technology*, 38(2), 89-104.
- [34] Montgomery, D. C. (2020). *Introduction to Statistical Quality Control* (8th ed.). Wiley.
- [35] Stevens, J. P., Zhan, A., & Duan, T. (2023). Detecting model drift in predictive algorithms for health care. *Journal of the American Medical Informatics Association*, 30(1), 19-29.